NANO LETTERS
Letter
pubs.acs.org/NanoLett

Dielectrophoresis-Assembled Zeolitic Imidazolate Framework Nanoparticle-Coupled Resonators for Highly Sensitive and Selective Gas Detection

Yongha Hwang,*,† Hyunmin Sohn,† Anh Phan,‡ Omar M. Yaghi,§ and Rob N. Candler†,∥

†Department of Electrical Engineering, University of California, Los Angeles, California 90095, United States
‡Molecular and NanoArchitecture Center, Ho Chi Minh, 721337, Vietnam
§Department of Chemistry, University of California, Berkeley, California 94720, United States
∥California NanoSystems Institute, University of California, Los Angeles, California 90095, United States

Supporting Information

ABSTRACT: This work reports on zeolitic imidazolate framework (ZIF)-coupled microscale resonators for highly sensitive and selective gas detection. The combination of microscale resonators and nanoscale materials simultaneously permits the benefit of larger capture area for adsorption from the resonator and enhanced surface adsorption capacity from the nanoscale ZIF structure. Dielectrophoresis (DEP) was demonstrated as a novel method for directly assembling concentrated ZIF nanoparticles on targeted regions of silicon resonant sensors. As part of the dielectrophoretic assembly process, the first ever measurements of the Clausius−Mossotti factor for ZIFs were conducted to determine optimal conditions for DEP assembly. The first ever real-time adsorption measurements of ZIFs were also performed to investigate the possibility of inherent gas selectivity. The ZIF-coupled resonators demonstrated sensitivity improvement up to 150 times over a bare silicon resonator with identical dimensions, and real-time adsorption measurements of ZIFs revealed different adsorption time constants for IPA and CO_2.

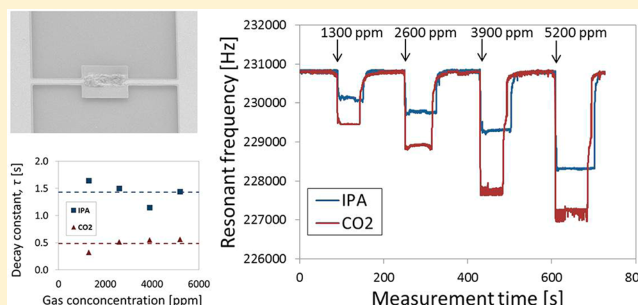

KEYWORDS: *Gas detectors, dielectrophoresis, decay constant, sensitivity, selectivity, zeolitic imidazolate framework*

A strong need exists for miniature chemical detection systems that can provide highly sensitive detection of multiple species (e.g., electronic noses). A number of resonant-based detection systems have been investigated for sensitive chemical and biological sensing, including QCM (quartz crystal microbalance),[1] SAW (surface acoustic wave),[2] or FBAR (film bulk acoustic resonator) platforms.[3] Miniaturization of resonators to the micro- and nanoscales have further been investigated, as their small mass enables a correspondingly small mass of adsorbed analytes to be detected.[4] Analyte detection is quantified by measuring the change in the resonant frequency of the resonator (Δf) due to the mass of adsorbed analytes (Δm):

$$\Delta f = -\frac{1}{2}\frac{f_0}{m}\Delta m \qquad (1)$$

where f_0 and m are the resonant frequency and mass, respectively, of the resonator without adsorbed analytes.[5] According to eq 1, a straightforward approach to increase Δf (i.e., the sensitivity) is to reduce device dimensions, since the ratio of f_0 to m increases with decreasing resonator size. Unfortunately, miniaturization has its limits; nanoscale resonators are more difficult to actuate and sense, and their reduced capture area increases the time required for a given mass of analytes to accumulate on the sensor surface.[6] An alternative approach for improving the sensitivity is to increase Δm (i.e., the number of analytes at the sensor surface). Analyte capture can be enhanced by increasing the available surface area through various functionalization methods[7] or porous treatment of the sensor surface.[5,8] While the enhanced sensitivity available in any porous material provides a path to measurements with fine resolution, an equally, if not more, important challenge is that of selective detection between different gases.

Selective detection generally requires chemical treatments to functionalize sensors, allowing them to bind analytes of interest.[9] Achieving selective detection with a single resonant sensor has traditionally been difficult because simply enhancing selectivity for a particular gas does not distinguish between a low concentration of the target gas and a high concentration of another gas (i.e., they would have the same Δf). Thus, multielement arrays are subjected to various chemical treatments to achieve selectivity. In this work, our approach assembles highly porous ZIF (zeolitic imidazolate frameworks)

Received: July 25, 2013
Revised: September 23, 2013
Published: October 7, 2013

 © 2013 American Chemical Society

nanoparticles to provide selectivity to desired analytes using adsorption time constants, which are determined by the ZIF and the particular analyte. In comparison with our previous report,[10] the unique contribution of this work is to assemble ZIF nanoparticles using dielectrophoresis and, more importantly, to analyze shift of the resonant frequency in terms of decaying constants using a feedback loop, enabling ZIF-coupled resonators to possess the path to selectivity. In other words, the method of pure scaling for improving only sensitivity has been developed significantly; however, the combination of sensitivity with selectivity is necessary for usable sensors. The combination of sensitivity and selectivity is the focus of this work.

A zeolitic imidazolate framework (ZIF) is a new class of three-dimensional crystalline structures with exceptional surface area and nanoporosity. ZIF-69 has a Langmuir surface area of 1070 m^2/g,[11] among the highest surface area used in adsorption-based sensing, and it exhibits a high affinity for CO_2 (1 L of ZIF-69 can store 49.2 L of CO_2 gas at 273 K).[12] Recently, ZIFs have been gaining attention for gas storage, filtering applications,[12,13] and sensing methodologies that detect changes in impedance, refractive index, strain, or speed of surface acoustic waves.[14−17] Previous work investigated ZIFs for gas detection by drop casting ZIFs onto designated regions of a resonator, thus achieving both the sensitivity of nanoscale devices and the capture area of microscale devices.[18] However, the drop casting process was labor-intensive, produced low yield, and more importantly led to agglomerated ZIFs, which obstructed the adsorption of gas onto internal layers of ZIFs and thus limited the sensitivity of the device. To maximize the sensitivity of the resonant sensor, the ZIF nanoparticles should ideally coat the sensor without obstructing the adsorption of gas. Unfortunately, conventional methods for positioning nanoparticles (e.g., direct growth,[19] catalyst,[20] bonding,[21] random spreading,[22] and nanomanipulation[23]) are not well-suited for coupling ZIFs to silicon resonators for several reasons. First, direct growth and catalyst techniques do not currently exist for ZIFs. Second, bonding techniques use adhesives that could coat ZIFs and limit their exposure to analytes in the environment. Finally, random spreading and nanomanipulation techniques sparsely distribute ZIFs, which minimizes the surface area available for gas adsorption. One technique that has not yet been explored for ZIF assembly is dielectrophoresis.

Dielectrophoresis (DEP) has been demonstrated as a simple and effective method to rapidly manipulate, sort, and assemble both biological and synthetic colloidal particles. When a nonuniform electric field is applied, the interfacial polarization between a particle and the media induces a dielectrophoretic force (F_{DEP}) on the particle:[24]

$$\langle F_{DEP} \rangle = 2\pi r^3 \varepsilon_m Re[CM] \nabla |E|^2 \quad (2)$$

$$Re[CM] = \frac{\varepsilon_p - \varepsilon_m}{\varepsilon_p - 2\varepsilon_m} \quad (3)$$

where r is the particle radius, $Re[CM]$ is real part of Clausius−Mossotti (CM) factor, ε_m is the permittivity of the media, ε_p is the permittivity of the particle, and E is the strength of the applied electric field. The CM factor (bounded by 1 and −0.5) is a measure of the degree of polarization and is a function of the particle's material properties and the frequency of the applied electric field.[25] The CM factor can be determined by measuring particle velocity as a function of frequency.[24] According to 2, a positive F_{DEP} is induced when $Re[CM] > 0$, attracting particles to regions of high electric field strength, such as the edge of an electrode. This positive force regime generally occurs at lower frequencies, depending on the relative permittivity of the particles with respect to the suspending medium. Conversely, at high frequencies, a negative F_{DEP} is induced ($Re[CM] < 0$), and particles are repelled to regions of low electric field strength. The frequency at which F_{DEP} transitions from positive to negative is called the crossover frequency. In this work, dielectrophoresis (DEP) is demonstrated as a novel method for directly assembling non-agglomerated ZIFs onto resonators.

To determine the optimal conditions for coupling ZIFs to silicon resonators, the crossover frequency and CM factor for ZIF-69 were experimentally determined (Figure 1). Coplanar

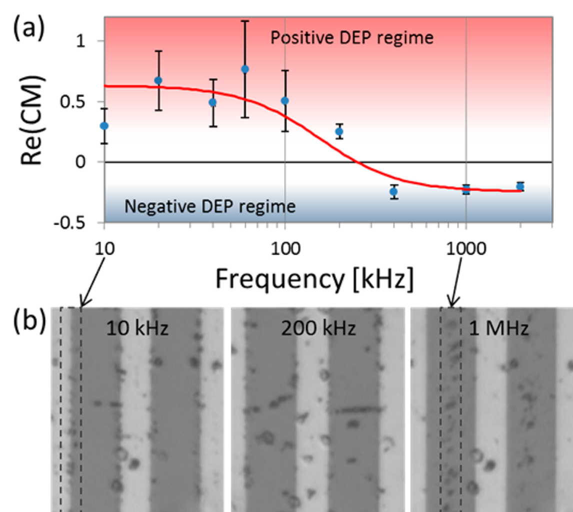

Figure 1. (a) Clausius−Mossotti (CM) factor as a function of frequency for ZIF-69 from 10 kHz to 2 MHz. Particle motions were recorded and the CM factors extracted. The crossover frequency for positive- and negative DEP is ∼250 kHz. (b) Coplanar electrodes (10 μm wide and with 15 μm spacing) with ZIF-69 particles at 10 kHz, 200 kHz, and 1 MHz suspended in DI water. The particles are attracted to the edges of the electrode by positive DEP (at 10 kHz). As the frequency is increased, the particles move away from electrodes (at 200 kHz) and are then repelled to the centers of the gap between electrodes by negative DEP (at 1 MHz).

electrodes generated DEP forces. A CCD camera captured video of particle motions at 59 frames/s, and particle motions were analyzed with IMAGEJ software.[26] At 10 kHz, ZIFs collected along the edges of the electrodes, indicating a positive F_{DEP}. As the frequency was increased to 200 kHz, ZIFs began to move away from the electrode edges, indicating a negative F_{DEP}. At 1 MHz, they accumulated between the electrodes, and some even levitated above the electrodes. In the transition between positive and negative DEP, some particles were observed to form chains along the electric field gradient lines due to interparticle electrostatic interactions.[27] From a global fit on the experimental curves according to eq 3, the $Re[CM]$ crossover for ZIF-69 occurred at ∼250 kHz. Applied voltage was below 5 V_{pp} to limit the electrothermal forces that might cause local flow disturbances.[24]

Based on experimental observation that resonators blanket-coated with ZIFs surprisingly showed an increase in resonant frequency during gas adsorption, the shift in resonant frequency

as a function of the stress induced by ZIF coatings was simulated using COMSOL (Figure 2). To isolate the role of stress, a negligible change in mass was assumed. Simulation results showed that tensile stress caused an increase in resonant frequency, while compressive stress caused a decrease in resonant frequency. Therefore, gas adsorption by ZIFs was determined to induce tensile stress in resonators. In addition, results showed that ZIFs should be assembled in targeted regions of the resonator, as opposed to blanket coating the entire resonator. Covering regions of high displacement would lead to surface stresses which could cause two deleterious effects, (1) counterbalancing the resonant frequency shift due to loaded mass on the devices[28,29] and (2) lowering the resonator quality factor due to surface-induced energy dissipation.[30] Therefore, it is desirable to control the location on the resonator where ZIFs are deposited, with ameliorating of stress-induced frequency shifts being particularly important.

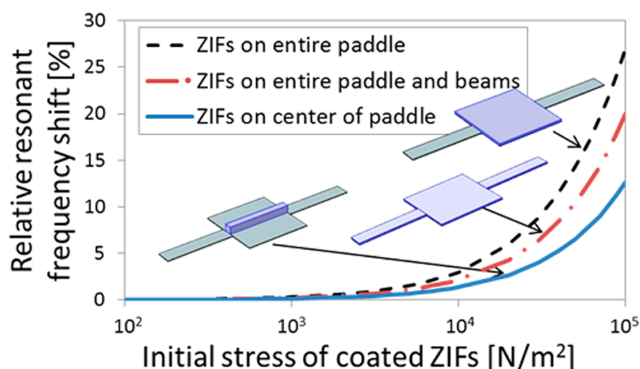

Figure 2. Simulated resonant frequency shift using COMSOL due to surface stress from ZIF coating. The resonators consist of a 450-nm-thick, 45-μm-long, 45-μm-wide center paddle fixed to anchors at each end through 450-nm-thick, 45-μm-long, 10-μm-wide torsional beams. ZIFs can induce tensile stress on the resonator, increasing its resonant frequency. Location of ZIFs on the resonator is important because frequency shift can vary by 126% for the same amount of ZIFs depending on the placement on the resonator. Increased resonant frequency from tensile stress counterbalances decrease in resonant frequency from adsorbed analytes, making increased stiffness undesirable. (Parts in purple represent assembled ZIFs on the resonator, and the same amount of ZIFs (1170 μm^3) is attached to each resonator).

The resonators were fabricated using a two-step sacrificial layer process in combination with standard surface micromachining processes, and DEP was used for assembling ZIFs. Unless otherwise specified, fabrication processes were carried out at room temperature. As shown in Figure 3, the process started with PECVD deposition at 250 °C of a 5.5-μm-thick layer of silicon dioxide (SiO_2) as the first sacrificial layer followed by LPCVD deposition at 600 °C of a 450-nm-thick polysilicon as a structural layer, all on a 4-in. (100) silicon wafer. The structural layer was patterned via photolithography and etched via deep reactive ion etching to define the resonators (Figure 3a). Resonators were designed to have a 450-nm-thick, 45-μm-long, 45-μm-wide center paddle fixed to anchors through 450-nm-thick, 45-μm-long, 10-μm-wide torsional beams. Chromium/gold layers were then deposited and patterned by lift-off photolithography to define the planar electrodes for generating the DEP force (Figure 3b). After protecting the electrodes with a photoresist (PR) passivation layer (Figure 3c), the SiO_2 sacrificial layer was removed by immersing wafers in 49% HF solution, followed by immersion in deionized (DI) water. Note that, since HF etches ZIFs, HF etching of the SiO_2 sacrificial layer must occur before DEP assembly of the ZIFs. To support the resonator during the assembly of ZIFs, a sacrificial PR support layer was exchanged with a *p*-dichlorobenzene (p-DCB) support layer, which prevented stiction (Figure 3d–f).[31] The PR layer plays dual roles, acting as both a second sacrificial layer for supporting the resonator and as a mold for localizing the ZIFs on top of the resonator during DEP assembly.

For the DEP assembly process (Figure 3g), ZIF-69 particles were sonicated in DI water for 15 min to ensure a uniform dispersion of ZIFs and then poured over the PR mold on the resonator. Next, a 5 V_{pp}, 10 kHz AC signal was applied via a function generator (Agilent 33220A) to the planar electrodes, generating a DEP force that collected the ZIFs on the electrodes of the center paddle. The AC voltage was applied until the DI water fully evaporated, after which the ZIFs were observed to adhere to the resonator surface, possibly as a result of van der Waals forces.[32] Once the ZIFs were assembled, the sacrificial PR was removed with acetone to release the ZIF-coupled resonator, and sublimation drying of p-DCB was performed again to avoid adhesion of the resonator to the underlying substrate (Figure 3h). Figure 4 shows fabricated silicon resonators with and without ZIFs.

The ZIF-coupled resonant gas sensors were tested at room temperature with a test setup that consisted of a Laser Doppler vibrometer (LDV, Polytec OFV-5000), an HP 8753D network analyzer, and a custom-built vacuum chamber, as shown in Figure 5. The network analyzer produced a driving frequency to stimulate the resonator. The LDV differentially detected resonator vibration using two laser signals, one focused on the resonator and the other focused on the anchor of the

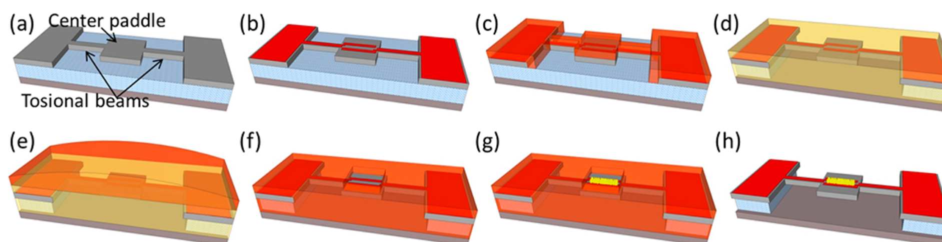

Figure 3. Fabrication process for ZIF-coupled resonator. (a) Patterning the body of the resonator. (b) Lift-off for planar electrodes. (c) Covering the metal electrodes with a passivation layer. (d) Etching the first sacrificial layer and filling p-DCB underneath the resonator. (e) Pouring thick photoresist over the solid p-DCB. (f) Reflowing the photoresist during sublimation of p-DCB and patterning it as the second sacrificial layer and mold for a target region of ZIF particles. (g) Assembling ZIF particles by DEP-induced attractive force. (h) Releasing the ZIF-coupled resonator.

dx.doi.org/10.1021/nl4027692 | *Nano Lett.* 2013, 13, 5271–5276

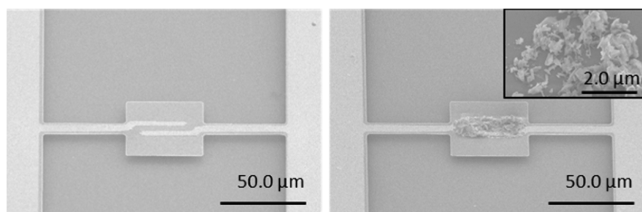

Figure 4. Tilted-view SEM images of the fabricated resonators without ZIFs (left) and with ZIFs (right). In the figure on the right, the inset shows ZIF-69 particles assembled on the surface of the resonator. The particles have random shapes less than 1 μm in diameter.

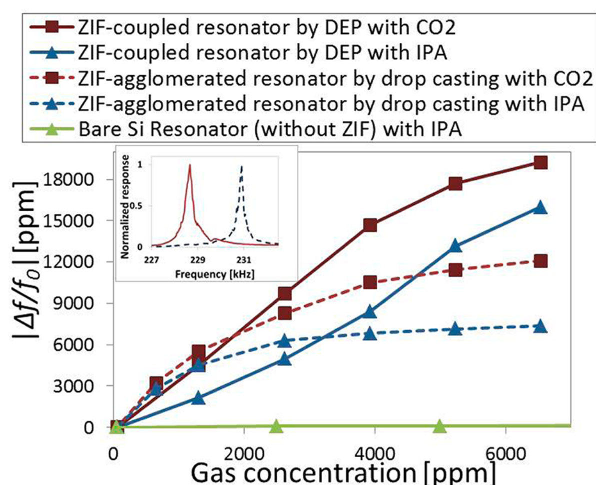

Figure 6. Responses of resonators with and without ZIFs as a function of IPA and CO_2 gas concentration. The ZIF-coupled resonator assembled by DEP shows higher sensitivity over a larger concentration range compared to the ZIF-agglomerated resonator assembled by drop casting. The bare Si resonator without ZIFs shows no response to gas. The inset is a set of frequency spectra showing change of resonant frequency by adsorption of 2500 ppm CO_2 (from dashed line to solid line). The measurements were performed via the open loop setup (Figure 5a).

resonator, and output a velocity proportional to the displacement of the resonator. The displacement magnitude and phase with respect to the driving frequency was then analyzed via the network analyzer in an open loop setup. The resonant frequency and quality factor could then be determined (Figure 5a). For real-time mass sensing, the resonator was placed in a feedback circuit that satisfied the loop gain and phase conditions for oscillation, and a frequency counter (Agilent 53220A) detected the resonant frequency from the self-oscillating signal (Figure 5b–c).[33]

Figure 6 shows the shift in resonant frequency ($\Delta f/f_0$) due to adsorption of different gases for silicon resonators with and without ZIF assembly. The resonant characteristics were measured using the open loop setup (Figure 5a). Whereas the frequency shifts of the bare silicon resonator without ZIFs were almost negligible upon exposure to IPA (isopropyl alcohol) gas, the resonant frequency of the ZIF-coupled resonator changed substantially due to the increase in surface area afforded by ZIFs. Inset shows a change in resonant frequency from 230.9 to 228.6 kHz with adsorption of 2500 ppm CO_2. The quality factor of the ZIF-coupled resonator was measured to be 1600 at room temperature. Quality factor was observed to be reduced typically by a factor of 2 after assembly of ZIFs, possibly due to surface-induced energy dissipation.[34]

The results of the DEP-assembled ZIF-coupled resonators were compared with those from a ZIF-agglomerated resonator fabricated through via drop casting, which was a labor-intensive process with lower yield.[18] As shown in Figure 6, the response of the ZIF-coupled resonator is much more linear compared to the ZIF-agglomerated resonator, whose response saturates over the same concentration range. The agglomerated ZIFs likely obstructed gas adsorption into internal layers of ZIFs, while the DEP-assembled ZIFs had increased exposure to the surrounding environment and could maximize contact with gas analytes. For different gases, the DEP-assembled ZIF-coupled resonator demonstrated from 0.8 to 1.6 times enhanced sensitivity compared to the ZIF-agglomerated resonator and from 56 to 158 times enhanced sensitivity compared to the bare silicon resonator without ZIFs. Furthermore, because of the inherent selectivity of ZIFs,[12] the ZIF-coupled resonator had higher sensitivity to CO_2 than IPA in spite of the lighter molar mass of CO_2. Uptake of a specific gas of ZIF-69 depends on pressure and temperature. Detailed properties were reported in the literature.[11−13] Assuming that the frequency shift is affected only by the mass change, the mass adsorbed on the ZIF-coupled resonator for a CO_2 concentration of 5200 ppm was calculated using eq 1 to be 99 pg. As an adsorbed areal mass of CO_2 is calculated as 28 ng/cm^2 for a monolayer,[13] a bare silicon resonator with surface area of 4900 μm^2 is expected to adsorb only 1.3 pg of CO_2. The amount of CO_2 adsorbed onto the ZIF-coupled resonator corresponds to 72 times more than the bare silicon resonator itself, which implies the adsorption of the ZIF-coupled resonator occurs not only on the surface but also within the ZIFs, as is desired. The results demonstrate the ability of ZIFs to increase the surface area available for gas detection, thus enhancing the sensitivity of the gas sensor.

Besides sensitivity, selectivity is an important property of gas sensors. The difference in time required to adsorb different

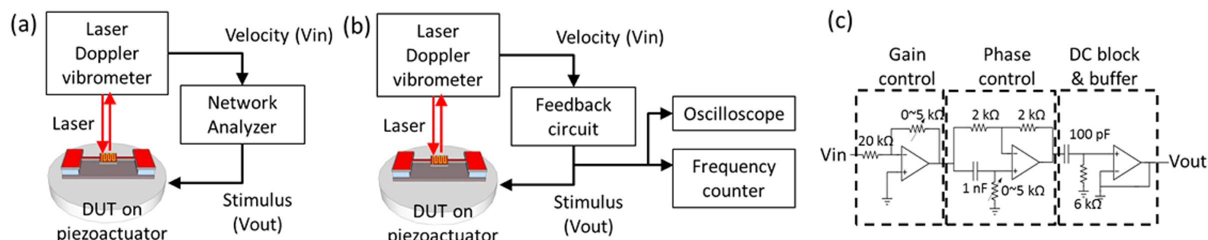

Figure 5. Measurement setups for the resonator characterization using a LDV. (a) The displacement magnitude of the resonator with respect to the driven frequency is analyzed with a network analyzer from the velocity output of the LDV. (b) For real-time mass sensing, the resonator is kept self-oscillating at its resonant frequency by providing a feedback circuit, and the resonant frequency is detected by a frequency counter. (c) The feedback circuit controls the signal gain and shifts the phase of the signal.

dx.doi.org/10.1021/nl4027692 | Nano Lett. 2013, 13, 5271−5276

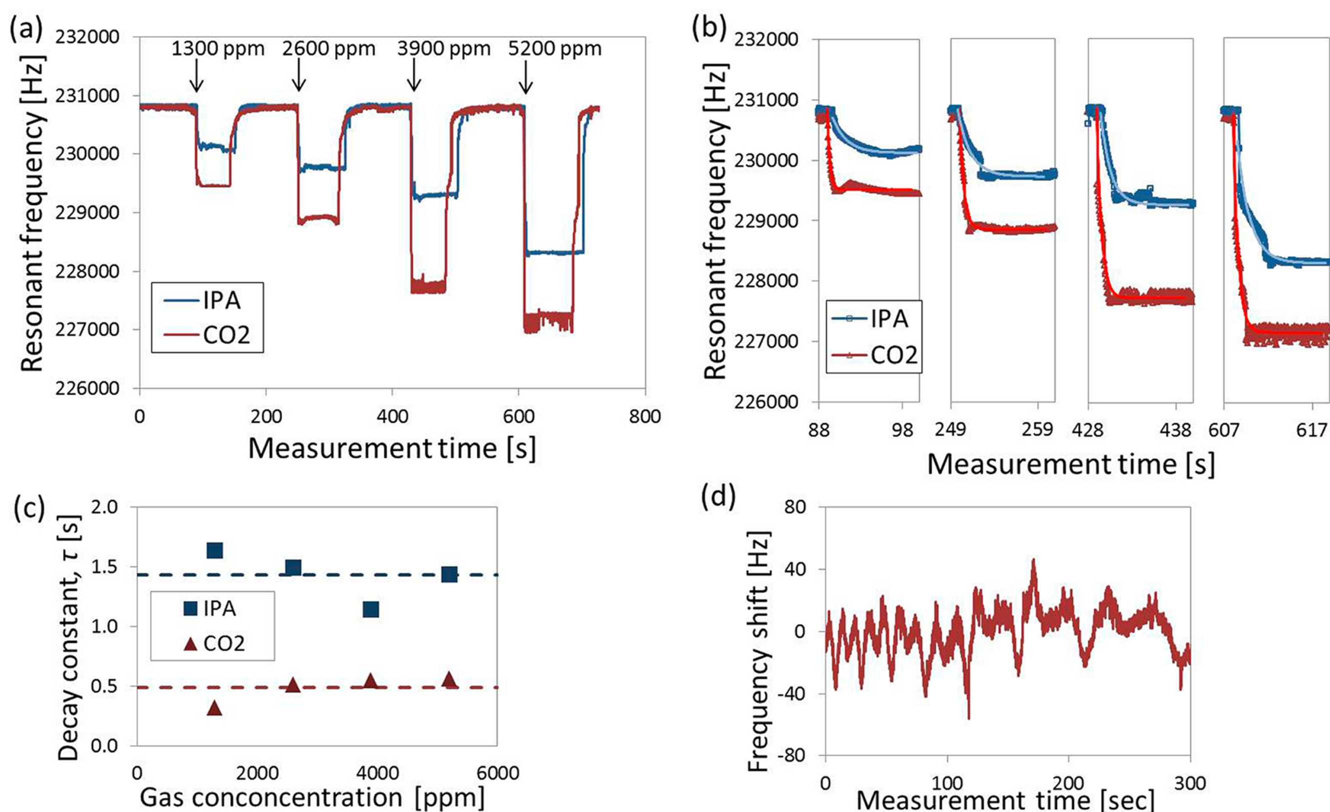

Figure 7. (a) Real-time gas sensing experiment with the ZIF-coupled resonator and (b) expanded view of the frequency drop from adsorption of IPA (blue) and CO_2 (red) with a sampling period of 50 ms. The experimental curves are fit to an exponential decay function (light blue and light red solid lines), and the fitting parameters are compared in Table 1. (c) The decay constants for IPA and CO_2 are 1.43 ± 0.28 s and 0.49 ± 0.17 s, respectively, demonstrating the potential to discern different gases based on adsorption time. (d) The Allan deviation is characterized over 500 s. The measured Allan deviation for τ = 1 s of reflects capability of ~26 fg mass resolution.

gases can be used to discern the selectivity of the sensor to these gases. In other words, the amplitude of the frequency shift and the decay constant of the adsorption time can provide information about concentration of specific gas molecules that have adsorbed onto the sensor, indicating chemical recognition ability of the ZIF-coupled resonator sensor. To measure the adsorption times, the ZIF-coupled resonator was exposed to a series of IPA or CO_2 gas pulses, and the resonant frequency was measured using the feedback loop setup for real-time mass sensing (Figure 5b−c). The resonant frequency decreased rapidly during the injection of gas and then recovered to its baseline values within 10 s upon removal of gas, indicating reversible adsorption (Figure 7a). Since the removal of gas was controlled manually, discharge rates are not informative, so only absorption dynamics were studied (see the Supporting Information). To quantify the time-dependent exponential decay of resonant frequency due to gas adsorption, the experimental data was fit to a global function, $f(t) = \Delta f \exp[-(t/\tau)]$, where Δf is the amplitude of frequency shift, and τ is the decay constant (Figure 7b). Table 1 compares the fit parameters, which depend on both the concentration of the arriving analyte and ZIF-69's selectivity to it. The decay constants were measured to be 1.43 ± 0.28 s and 0.49 ± 0.17 s for IPA and CO_2, respectively (Figure 7c). The smaller decay constant for CO_2 indicates an inherent selectivity of ZIF-69 to CO_2 compared to IPA. Regarding measurement resolution, the Allan deviation of the resonant frequency is 4.7 ppm over a 1 s integration time (Figure 7d). Temperature-induced frequency drift for silicon resonators is one possible noise source.[35]

Table 1. Fitting Parameters of Time-Dependent Exponential Decay of the Resonant Frequency due to Different Concentrations of IPA and CO_2

	IPA		CO_2	
gas concentration (ppm)	frequency shift, Δf (Hz)	decay constant, τ (s)	frequency shift, Δf (Hz)	decay constant, τ (s)
1300	606.64	1.64	1460.54	0.32
2600	1110.26	1.49	2246.66	0.51
3900	1519.30	1.14	3547.28	0.55
5200	2203.10	1.44	3629.07	0.56

Coupling a layer of ZIFs creates a bimorph type structure, which could potentially impact the frequency as a function of temperature. However, based on finite element simulations considering a mismatch of thermal expansion of coupled ZIFs, the addition of ZIFs will impact ~0.87% of the temperature coefficient of frequency (TCf) (see the Supporting Information). The similarity in TCf for coated and uncoated resonators can be partially attributed to the targeted placement ZIFs, whose location was chosen to minimize the impact of stress, as previously mentioned.

The minimum detectable mass is calculated as $\delta M = 2m_{\mathrm{eff}}\langle \delta f/f_0\rangle_\tau$,[36] where m_{eff} (~2.8×10^{-9} g) is the effective mass by means of Rayleigh's principle,[37] and $\langle \delta f/f_0\rangle_\tau$ is the measured Allan deviation of the resonator. Hence, the limit of detection of the ZIF-coupled resonator for gas sensing is ~26 fg.

In summary, DEP-assembled ZIF-coupled microresonators have demonstrated sensitivity improvement up to 150 times over bare silicon resonators with identical dimensions, as the combination of microscale resonators and nanoscale materials simultaneously permits the benefit of larger capture area for adsorption from the resonator and enhanced surface adsorption capacity from the nanoscale ZIF structure. Also, real-time adsorption data revealed the different adsorption time constants of IPA and CO_2. These real-time adsorption measurements in ZIFs demonstrate the possibility of inherent gas selectivity for these sensors that could be tuned by the choice of ZIFs. Additionally, the DEP-assembly method combined with the two-step sacrificial layer fabrication process can be used to assemble a diverse class of nanomaterials on resonant sensors, opening the door for a wide variety of adsorption-based sensing applications.

■ ASSOCIATED CONTENT

Ⓢ Supporting Information

Figures showing expanded view of the frequency recovery from removal of analytes and simulated temperature characteristics. This material is available free of charge via the Internet at http://pubs.acs.org.

■ AUTHOR INFORMATION

Corresponding Author

*E-mail: hwangyongha@ucla.edu.

Notes

The authors declare no competing financial interest.

■ ACKNOWLEDGMENTS

This work was supported by the Broadening Participation Research Initiation Grants program of the National Science Foundation under award no. 0926228 and by the Focus Center for Functional Engineered Nano Architectonics. We would also like to gratefully thank Prof. Kos Galatsis and Prof. Katherine Candler for helpful discussions. Device fabrication was performed in the Nano-electronics Research Facility (NRF) at UCLA.

■ REFERENCES

(1) Sun, P.; Jiang, Y. D.; Xie, G. Z.; Du, X. S.; Hu, J. *Sens. Actuators, B* **2009**, *141* (1), 104−108.

(2) Wen, W.; He, S. T.; Li, S. Z.; Liu, M. H.; Yong, P. *Sens. Actuators, B* **2007**, *125* (2), 422−427.

(3) Penza, M.; Aversa, P.; Cassano, G.; Suriano, D.; WIodarski, W.; Benetti, M.; Cannata, D.; Di Pietrantonio, F.; Verona, E. *IEEE Trans. Electron Dev.* **2008**, *55* (5), 1237−1243.

(4) Waggoner, P. S.; Craighead, H. G. *Lab Chip* **2007**, *7* (10), 1238−1255.

(5) Lee, D.; Shin, N.; Lee, K. H.; Jeon, S. *Sens. Actuators, B* **2009**, *137* (2), 561−565.

(6) Sheehan, P. E.; Whitman, L. J. *Nano Lett.* **2005**, *5* (4), 803−807.

(7) Braun, T.; Ghatkesar, M. K.; Backmann, N.; Grange, W.; Boulanger, P.; Letellier, L.; Lang, H. P.; Bietsch, A.; Gerber, C.; Hegner, M. *Nat. Nanotechnol.* **2009**, *4* (3), 179−185.

(8) Xu, P. C.; Yu, H. T.; Li, X. X. *Anal. Chem.* **2011**, *83* (9), 3448−3454.

(9) Arntz, Y.; Seelig, J. D.; Lang, H. P.; Zhang, J.; Hunziker, P.; Ramseyer, J. P.; Meyer, E.; Hegner, M.; Gerber, C. *Nanotechnology* **2003**, *14* (1), 86−90.

(10) Hwang, Y.-H.; Phan, A.; Galatsis, K.; Yaghi, O. M.; Candler, R. N. ZIF-coupled microresonator for highly sensitive and selective gas detection. In *The 16th International Conference on Miniaturized Systems for Chemistry and Life Sciences (MicroTAS)*, Okinawa, Japan, Oct 28−Nov 1, 2012.

(11) Phan, A.; Doonan, C. J.; Uribe-Romo, F. J.; Knobler, C. B.; O'Keeffe, M.; Yaghi, O. M. *Acc. Chem. Res.* **2010**, *43* (1), 58−67.

(12) Banerjee, R.; Phan, A.; Wang, B.; Knobler, C.; Furukawa, H.; O'Keeffe, M.; Yaghi, O. M. *Science* **2008**, *319* (5865), 939−943.

(13) Furukawa, H.; Ko, N.; Go, Y. B.; Aratani, N.; Choi, S. B.; Choi, E.; Yazaydin, A. O.; Snurr, R. Q.; O'Keeffe, M.; Kim, J.; Yaghi, O. M. *Science* **2010**, *329* (5990), 424−428.

(14) Lu, G.; Hupp, J. T. *J. Am. Chem. Soc.* **2010**, *132* (23), 7832−7833.

(15) Allendorf, M. D.; Houk, R. J. T.; Andruszkiewicz, L.; Talin, A. A.; Pikarsky, J.; Choudhury, A.; Gall, K. A.; Hesketh, P. J. *J. Am. Chem. Soc.* **2008**, *130* (44), 14404.

(16) Achmann, S.; Hagen, G.; Kita, J.; Malkowsky, I. M.; Kiener, C.; Moos, R. *Sensors* **2009**, *9* (3), 1574−1589.

(17) Robinson, A. L.; Stavila, V. L.; Zeitler, T. R.; White, M. I.; Thornberg, S. M.; Greathouse, J. A.; Allendorf, M. D. *Anal. Chem.* **2012**, *84* (16), 7043−7051.

(18) Hwang, Y. H.; Phan, A.; Galatsis, K.; Yaghi, O. M.; Candler, R. N. ZIF-coupled microresonator for highly sensitive and selective gas detection. In *Proceedings of Conference on Miniaturized Systems for Chemistry and Life Science (MicroTAS 2012)*, Okinawa, Japan, Oct 28−Nov 1, 2012; pp 231−233.

(19) Franklin, N. R.; Li, Y. M.; Chen, R. J.; Javey, A.; Dai, H. J. *Appl. Phys. Lett.* **2001**, *79* (27), 4571−4573.

(20) Cantoro, M.; Hofmann, S.; Pisana, S.; Scardaci, V.; Parvez, A.; Ducati, C.; Ferrari, A. C.; Blackburn, A. M.; Wang, K. Y.; Robertson, J. *Nano Lett.* **2006**, *6* (6), 1107−1112.

(21) Wang, N.; Bowers, B. J.; Arnold, D. P. *J. Appl. Phys.* **2008**, *103* (7), 07E109.

(22) Martel, R.; Schmidt, T.; Shea, H. R.; Hertel, T.; Avouris, P. *Appl. Phys. Lett.* **1998**, *73* (17), 2447−2449.

(23) Lixin, D.; Kaiyu, S.; Frutiger, D. R.; Subramanian, A.; Li, Z.; Nelson, B. J.; Xinyong, T.; Xiaobin, Z. *IEEE Transactions on Nanotechnology* **2008**, *7* (4), 508−517.

(24) Honegger, T.; Berton, K.; Picard, E.; Peyrade, D. *Appl. Phys. Lett.* **2011**, *98* (18), 181906−3.

(25) Green, N. G.; Morgan, H. *J. Phys. Chem. B* **1999**, *103* (1), 41−50.

(26) Sbalzarini, I. F.; Koumoutsakos, P. *J. Struct. Biol.* **2005**, *151* (2), 182−195.

(27) Hoffman, P. D.; Zhu, Y. X. *Appl. Phys. Lett.* **2008**, *92* (22), 224103.

(28) Chen, G. Y.; Thundat, T.; Wachter, E. A.; Warmack, R. J. *J. Appl. Phys.* **1995**, *77* (8), 3618−3622.

(29) McFarland, A. W.; Poggi, M. A.; Doyle, M. J.; Bottomley, L. A.; Colton, J. S. *Appl. Phys. Lett.* **2005**, *87* (5), 053505.

(30) Yang, J. L.; Ono, T.; Esashi, M. *J. Vac. Sci. Technol., B* **2001**, *19* (2), 551−556.

(31) Hwang, Y.; Candler, R. N. *J. Microelectromech. Syst.* **2012**, *21* (6), 1282−1284.

(32) Hartley, P. A.; Parfitt, G. D.; Pollack, L. B. *Powder Technol.* **1985**, *42* (1), 35−46.

(33) Park, K.; Kim, N.; Morisette, D. T.; Aluru, N. R.; Bashir, R. *J. Microelectromech. Sys.* **2012**, *21* (3), 702−711.

(34) Wang, Y.; Henry, J. A.; Zehnder, A. T.; Hines, M. A. *J. Phys. Chem. B* **2003**, *107* (51), 14270−14277.

(35) Tudor, M. J.; Andres, M. V.; Foulds, K. W. H.; Naden, J. M. *IEEE Proc. D: Control Theory Appl.* **1988**, *135* (5), 364−368.

(36) Forsen, E.; Abadal, G.; Ghatnekar-Nilsson, S.; Teva, J.; Verd, J.; Sandberg, R.; Svendsen, W.; Perez-Murano, F.; Esteve, J.; Figueras, E.; Campabadal, F.; Montelius, L.; Barniol, N.; Boisen, A. *Appl. Phys. Lett.* **2005**, *87* (4), 43507.

(37) Lobontiu, N.; Ilic, B.; Garcia, E.; Reissman, T.; Craighead, H. G. *Rev. Sci. Instrum.* **2006**, *77* (7), 073301−9.